Supplementary Materials

Persistent dysoxia in very shallow seas across the Late Cambrian SPICE Event in the Durness Group, UK

Ke Feng[1], Fred Bowyer[1,2], Andrew Curtis[1], Simon W. Poulton[2], Laetitia Pichevin[1], and Rachel Wood[1]

Methods

Sample preparation

Samples were halved with a diamond saw in order to retain archive material, and weathered surfaces were removed from one half. The samples were washed and dried at 40°C. Samples with visible signs of alteration and/or veining were rejected at this point. Halved samples were crushed and pulverised to homogeneous powder (<60 μm) using a tungsten carbide TEMA.

Total digestion

After ashing at 550°C for 8 h, samples were quantitatively dissolved in trace metal grade HNO_3, HF and $HClO_4$, heated in open PTFE cups and left to dry fully over a period of 24 h before addition of H_3BO_3 to prevent the formation of Al complexes. Dry residues were then dissolved in concentrated HNO_3 and diluted with ultrapure 18MΩ H_2O. Major element concentrations were analysed using inductively coupled plasma optical emission spectrometry (ICP-OES, Thermo Fisher iCAP 7400), and trace element concentrations were measured using inductively coupled plasma mass spectrometry (ICP-MS, Thermo Fisher

iCAPQc) at the School of Earth and Environment, University of Leeds. Total digestions of a standard material (SBC-1, United States Geological Survey) yielded values within the certified range for all elements analysed (<4%).

Fe speciation

Iron speciation analyses followed the established, operationally-defined method of Poulton and Canfield (2005), as modified in Poulton (2021). An initial leach targeting iron bound in carbonate phases (Fe_{carb}) employed Na-acetate, buffered to pH 4.5 with acetic acid and agitated at 50°C for 48 h. This was followed by a 2 h iron (oxyhydr)oxide (Fe_{ox}) extraction in Na-dithionite buffered to pH 4.8, and then a final extraction of magnetite (Fe_{mag}) with ammonium oxalate for 6 h. All steps of the sequential leach were performed at the Cohen Laboratories, University of Leeds, and resultant solutions were analysed for Fe using a Thermo Scientific iCE-3000 series flame atomic absorption spectrometer, with replicate extractions for each step yielding relative standard deviations (RSDs) of <5%. To ensure accuracy, Fe speciation reference material (WHIT) (Alcott et al., 2020) was run alongside each batch.

The concentration of pyrite iron (Fe_{py}) was determined through a boiling chromous chloride [$Cr(II)Cl_2$] distillation with a pre-leach in boiling 6 M HCl for quantitative extraction of acid volatile sulfide (AVS). Pre-leaching confirmed that no acid volatile sulfide was present. Weight percent Fe_{py} was determined gravimetrically after stoichiometric precipitation of Ag_2S.

I/(Ca + Mg)

Measurement of I/(Ca+Mg) ratios followed the procedure of Lu et al. (2010, 2016). 100 mg of powder was washed with 18 MΩ H_2O and dried at 40°C for 48 h. 5 mg of resultant powder was weighed for analysis. Samples were digested with 3% HNO_3. Iodine was stabilised with 3% ammonium hydroxide to create a mother solution. This was made to volume with a matrix solution of 3% HNO_3 + 0.5% ammonium hydroxide + 3% methanol. The solution was diluted with matrix to produce 50 ± 5 µg/ml Ca concentrations in each sample. Ca and Mg concentrations were measured using inductively coupled plasma-optical emission spectrometer (ICP-OES, Varian Vista Pro ICP-OES) and I concentrations were measured using inductively coupled plasma-mass spectrometer (High-resolution single collector ICP-MS, AttoM) at the University of Edinburgh, using a Tellurium internal standard. JCP-1 coral standard was analyzed as a reference material with RSDs < 4%.

Elemental enrichment factors

Enrichment factors (EF) provide a quantification of the level of accumulation of redox-sensitive trace metals (Algeo et al., 2009; Tribovillard et al., 2012), and EFs are commonly calculated for siliciclastic sediments by the following:

$$Element_{EF} = \frac{Element/Al}{Element_{UCC}/Al_{UCC}} \quad (1)$$

where UCC represents upper continental crust (here, we use concentrations from Gaschnig et al. (2016) except for Re, which is not reported, for which we use values of Chen et al.

(2016). However, utilizing EF values in sediments rich in carbonates is problematic, as low Al concentrations in such sediments result in elevated EFs relative to siliciclastic sediments (Tribovillard et al., 2006). This may be navigated by calculating elemental excess concentrations (Krewer et al., 2024), which are calculated by the following:

$$Element_{Excess} = Element_{Sample} - (Al_{Sample} \times \frac{Element_{UCC}}{Al_{UCC}}) \quad (2)$$

These values are then used to calculate revised EF values (EF^*) for carbonate-rich lithologies (*33*):

$$Element_{EF}{}^{*} = \frac{Element_{Excess} + Element_{UCC}}{Element_{UCC}} \quad (3)$$

Utilising EF^* allows the assessment of elemental enrichment factors in carbonate rocks and furthermore facilitates comparison to siliciclastic lithologies.

Redox Proxy Systematics

We deploy a multi-proxy approach to assess the redox evolution of the Eilean Dubh Formation. Fe speciation facilitates the assessment of redox conditions by measuring the concentration of Fe_{HR} (that is, a highly reactive Fe pool composed of Fe in carbonate and oxide minerals, magnetite, and pyrite - Fe_{Carb}, Fe_{Ox}, Fe_{Mag}, and Fe_{py}) and normalising these data to Fe_T (the total concentration of Fe within a sample) (Poulton and Canfield, 2005, 2011). Fe speciation has been calibrated in a variety of modern and ancient settings and is able to constrain 'oxic' and 'anoxic' conditions (Poulton, 2021; Poulton and Canfield, 2011; Raiswell et al., 2018), whereby ratios ≤0.22 are commonly indicative of oxic water column conditions. Ratios ≥0.38 are commonly indicative of precipitation of Fe–bearing

unsulfidised mineral phases and Fe sulfides under anoxic water column conditions in ferruginous and euxinic settings, respectively (Poulton and Raiswell, 2002; Poulton et al., 2004). These absolute thresholds may not be applicable to all depositional environments (e.g., high rates of deposition may obscure anoxic signals due to decreased Fe_{HR}/Fe_T values or mineral transformation during diagenesis) and as such, an equivocal zone is defined between these thresholds (Poulton and Canfield, 2011). Fe_T/Al ratios may be used to further assess redox conditions in the case of obscured values due to diagenesis. Values >0.66 are indicative of deposition under anoxic waters, with a typical oxic range of 0.44–0.66 (Clarkson et al., 2014).

Anoxic ferruginous and euxinic conditions may be distinguished by the proportion of pyrite-bound Fe (Fe_{Py}) within the Fe_{HR} pool, whereby values >0.8 are indicative of deposition under a euxinic water column (Poulton and Canfield, 2011). The potential for addition of Fe_{HR} into carbonates during diagenesis means that care must be taken when analysing carbonates for Fe speciation. Calibration of Fe speciation data from carbonates suggests that samples with Fe_T >0.5 wt% may record robust results, providing no deep burial dolomitisation has occurred (Clarkson et al., 2014). Fe speciation is, however, best deployed in addition to other proxies for water column redox conditions (Poulton, 2021), and therefore, we employ such a strategy by undertaking analysis of redox-sensitive trace elements and I/(Ca+Mg) ratios to more accurately constrain redox conditions in the Eilean Dubh Formation.

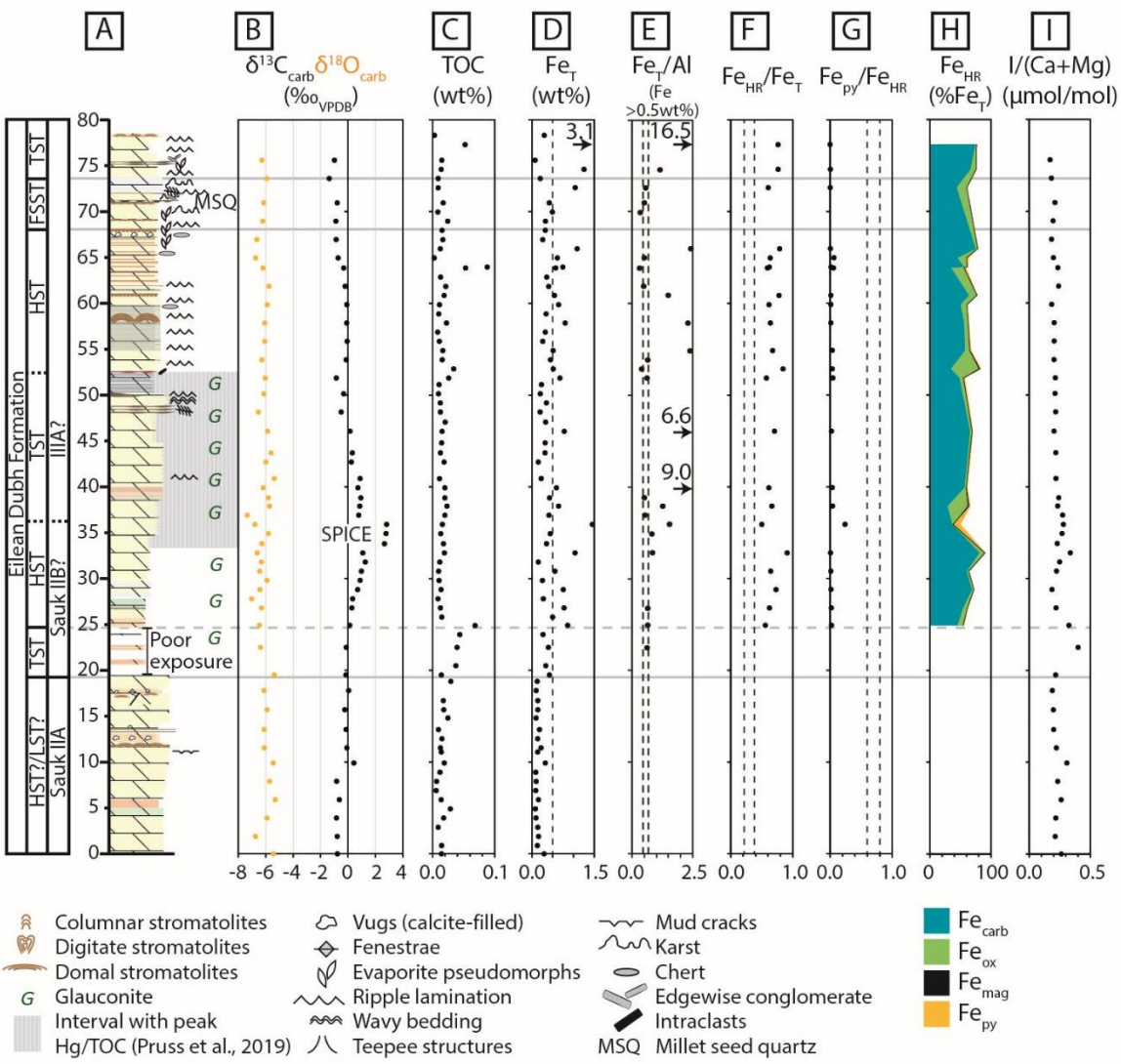

Figure S1. ***Expanded summary of redox dynamics through the late Cambrian SPICE event, recorded by the Eilean Dubh Formation*** *(A) Composite stratigraphy (modified from Raine, 2010). Horizontal grey dashed line marks Maximum Flooding Surface. TST = Transgressive Systems Tract. HST = Highstand Systems Tract. FSST = Falling Stage Systems Tract. (B) C isotope ($\delta^{13}C_{carb}$)and O isotope ($\delta^{18}O_{carb}$) record (this study). (C) Total organic carbon (TOC). (D) Total Fe concentration (Fe_T), with vertical dashed line marking the minimum threshold concentration of 0.5 wt% required to employ Fe speciation in carbonate-rich sedimentary rocks (Clarkson et al., 2014). (E) Fe_T/Al for samples with >0.5 wt% Fe_T. Vertical dashed lines in (E) bracket the range of normal oxic values in both carbonates and shales (0.44–0.66, Clarkson et al., 2014). (F) Fe_{HR}/Fe_T ratios. Vertical dashed lines in (F) represent empirically-derived 'oxic' (<0.22) and 'anoxic' (>0.38) threshold ratios separated by an equivocal zone (Poulton and Canfield, 2011). (G) Fe_{Py}/Fe_{HR} ratios, with vertical dashed lines representing the empirically-derived ferruginous (<0.60) and euxinic (>0.80) thresholds, separated by an equivocal zone that may represent euxinia (Poulton, 2021). (H) Fe speciation data, showing Fe phase concentrations as a proportion of Fe_T. (I) I/(Ca + Mg).*

Redox-sensitive trace element concentrations may be used to provide further constraints on redox conditions in modern and ancient settings (Calvert and Pedersen, 1993; Crusius et al., 1996; Tribovillard et al., 2006, 2012). Of particular note are the behaviours of U, Mo and Re. Under oxic conditions, Mo and U behave conservatively and occur primarily as MoO^{2-}_4 and $UO_2(CO_3)^{4-}_3$, with oxidation states Mo(VI) and U(VI) (Tribovillard et al., 2006). Under reducing conditions, U(VI) is reduced to insoluble U(IV), resulting in enrichments in the sedimentary record (Anderson et al., 1989). Mo is moderately enriched under reducing conditions, but becomes significantly enriched in the presence of free sulfide and is 'activated' at a critical HS^- activity to form thiomolybdates ($MoO_xS^{2-}_{4-x}$) (Helz et al., 1996). Mo concentrations may also be enriched by the function of a Mn-Fe particulate shuttle, whereby Mn-Fe (oxyhydr)oxides adsorb molybdate oxyanions, transporting them to the sediment-water interface (Algeo et al., 2009). Calibration in modern and ancient settings means that enrichments in Mo and U can be used to assess the redox state of the depositional environment and whether a particulate shuttle is active (Tribovillard et al., 2012). In oxic settings, Re is present as soluble Re(VII) and is reduced to insoluble Re(IV) under dysoxic conditions (Crusius et al., 1996). Re enrichment is considered to be a reliable indicator of dysoxic conditions due to accumulation in the sediment at O_2 penetration depths of $< \sim 1$ cm (Morford et al., 2005).

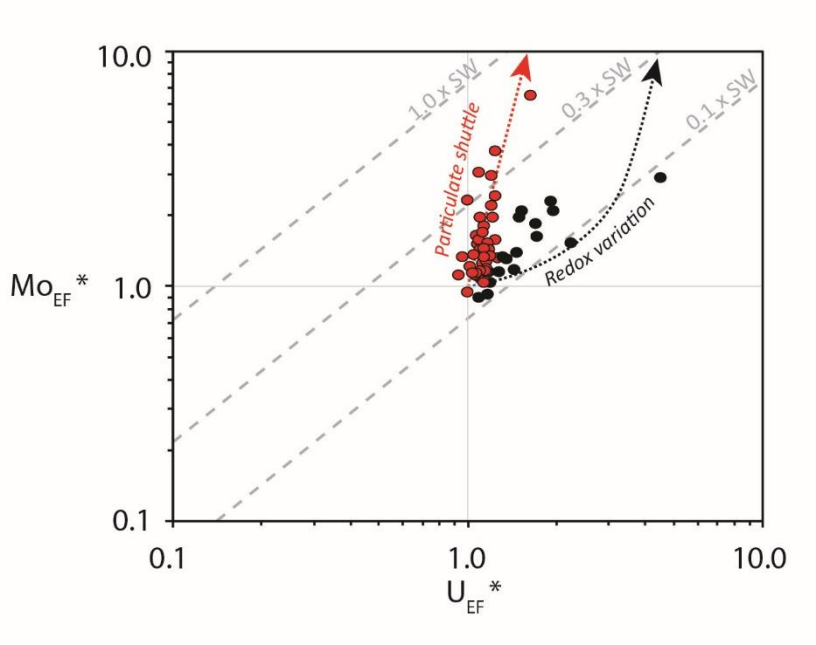

143

144 **Figure S2.** ***Cross-plot of revised Mo and U enrichment factors for carbonate samples of***

145 ***the Eilean Dubh Formation.***

146

147 I/(Ca+Mg) ratios in carbonates are commonly used to assess redox conditions due to the

148 sensitivity of I to redox conditions in seawater (Lu et al., 2010; Wong and Brewer, 1977).

149 The technique exploits the incorporation of oxidised iodate (IO_3^-) into the calcite and

150 dolomite crystal lattice in place of the carbonate (CO_3^{2-}) ion. It has been shown

151 experimentally that reduced iodide (I^-) does not similarly substitute for the carbonate ion and

152 thus iodine concentrations may be used to assess redox conditions (Lu et al., 2010). Iodine

153 has a high oxidation potential, similar to Mn, and is therefore sensitive to intermediate

154 oxygen concentrations (Lu et al., 2010, 2020). The proxy has been calibrated in a variety of

155 modern and ancient settings and is thus able to assess ancient redox conditions (Hardisty et

156 al., 2014, 2017; He et al., 2024; Lu et al., 2010, 2017, 2020). Some studies suggest that

I/(Ca+Mg) ratios may be used as proxies for absolute oxygen concentrations and that I/(Ca+Mg) values < 2.5-3 µmol/mol in modern foraminiferal samples indicate formation under dysoxic conditions (Huang et al., 2022; Lu et al., 2010, 2016). However, defining absolute concentrations may be complicated. Low I/(Ca+Mg) values have been reported in the presence of oxic waters due to the slow kinetics of iodide oxidation (Lu et al., 2020), and diagenesis has been shown to reduce I/(Ca+Mg) values (Hardisty et al., 2017). Major increases and decreases in I/(Ca+Mg) values are, however, robust indicators of elevated and depleted oxygen concentrations in seawater. Here, we interpret our data as such. Indeed, we therefore do not include the commonly reported suboxic-dysoxic threshold of 0.5 µmol/mol and refer to values between 0 and 2.6 as 'dysoxic' (i.e., with limited oxygen availability).

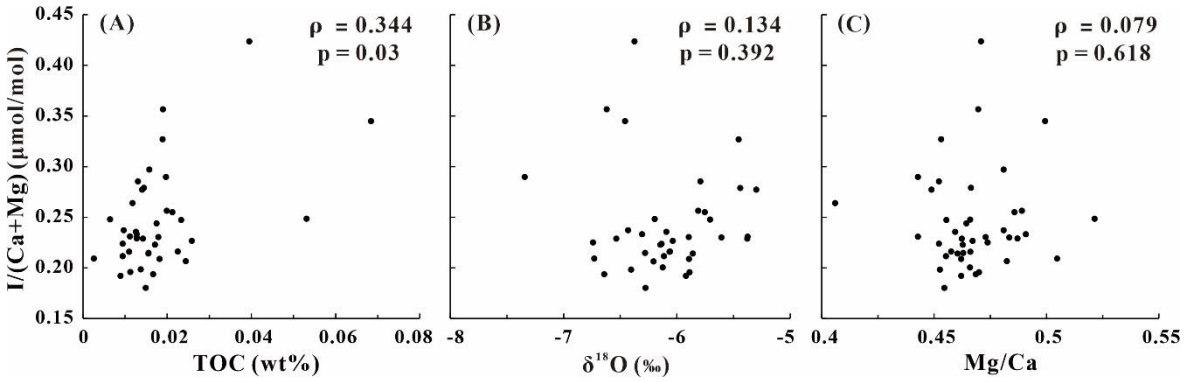

Figure S3. *Cross plots between I/(Ca+Mg) ratios and (A) TOC; (B) $\delta^{18}O$ and (C) Mg/Ca, with Spearman's rank and p-values.*

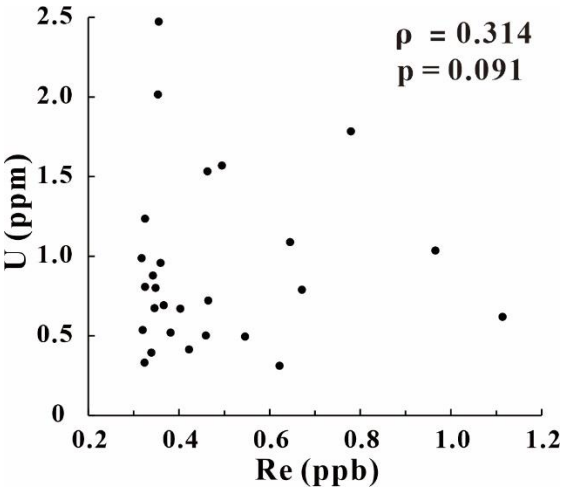

Figure S4. *Cross plot between U and Re, with Spearman's rank and p-values.*

References

L. J. Alcott, A. J. Krause, E. U. Hammarlund, C. J. Bjerrum, F. Scholz, Y. Xiong, A. J. Hobson, L. Neve, B. J. W. Mills, C. März, B. Schnetger, A. Bekker, S. W. Poulton, Development of Iron Speciation Reference Materials for Palaeoredox Analysis. Geostandards and Geoanalytical Research 44, 581–591 (2020).

T. J. Algeo, N. Tribovillard, Environmental analysis of paleoceanographic systems based on molybdenum–uranium covariation. Chemical Geology 268, 211–225 (2009).

R. F. Anderson, M. Q. Fleisher, A. P. LeHuray, Concentration, oxidation state, and particulate flux of uranium in the Black Sea. Geochimica et Cosmochimica Acta 53, 2215–2224 (1989).

Calvert, S.E. and Pedersen, T.F., 1993. Geochemistry of Recent oxic and anoxic marine sediments: Implications for the geological record. In: R.J. Parkes, P. Westbroek and J.W. de Leeuw (Editors), Marine Sediments, Burial, Pore Water Chemistry, Microbiology and Diagenesis. Mar. Geol., 113: 67-88.

Chen, K., Walker, R. J., Rudnick, R. L., Gao, S., Gaschnig, R. M., Puchtel, I. S., Tang, M., Hu, Z. C. (2016). Platinum-group element abundances and Re-Os isotopic systematics of the upper continental crust through time: Evidence from glacial diamictites. Geochimica et Cosmochimica Acta, 191, 1-16.

M. O. Clarkson, S. W. Poulton, R. Guilbaud, R. A. Wood, Assessing the utility of Fe/Al and

Fe-speciation to record water column redox conditions in carbonate-rich sediments. Chemical Geology 382, 111–122 (2014).

J. Crusius, S. Calvert, T. Pedersen, D. Sage, Rhenium and molybdenum enrichments in sediments as indicators of oxic, suboxic and sulfidic conditions of deposition. Earth and Planetary Science Letters 145, 65–78 (1996).

R. M. Gaschnig, R. L. Rudnick, W. F. McDonough, A. J. Kaufman, J. W. Valley, Z. Hu, S. Gao, M. L. Beck, Compositional evolution of the upper continental crust through time, as constrained by ancient glacial diamictites. Geochimica et Cosmochimica Acta 186, 316–343 (2016).

D. S. Hardisty, Z. Lu, N. J. Planavsky, A. Bekker, P. Philippot, X. Zhou, T. W. Lyons, An iodine record of Paleoproterozoic surface ocean oxygenation. Geology 42, 619–622 (2014).

D. S. Hardisty, Z. Lu, A. Bekker, C. W. Diamond, B. C. Gill, G. Jiang, L. C. Kah, A. H. Knoll, S. J. Loyd, M. R. Osburn, N. J. Planavsky, C. Wang, X. Zhou, T. W. Lyons, Perspectives on Proterozoic surface ocean redox from iodine contents in ancient and recent carbonate. Earth and Planetary Science Letters 463, 159–170 (2017).

R. He, A. Pohl, A. Prow, G. Jiang, C. C. Huan, M. R. Saltzman, Z. Lu, The dynamic ocean redox evolution during the late Cambrian SPICE: Evidence from the I/Ca proxy. *Global and Planetary Change* **233**, 104354 (2024).

G. R. Helz, C. V. Miller, J. M. Charnock, J. F. W. Mosselmans, R. A. D. Pattrick, C. D. Garner, D. J. Vaughan, Mechanism of molybdenum removal from the sea and its concentration in black shales: EXAFS evidence. Geochimica et Cosmochimica Acta 60, 3631–3642 (1996).

K. Huang, M. Cheng, T. J. Algeo, J. Hu, H. Wang, Z. Zhang, M. S. Dodd, Y. Wu, W. Guo, C. Li, Interaction of Shibantan Biota and environment in the terminal Ediacaran ocean: Evidence from I/(Ca+Mg) and sulfur isotopes. Precambrian Research 379, 106814 (2022).

C. Krewer, S. W. Poulton, R. J. Newton, C. März, B. J. W. Mills, T. Wagner, Controls on the Termination of Cretaceous Oceanic Anoxic Event 2 in the Tarfaya Basin, Morocco. American Journal of Science 324, 11 (2024).

W. Lu, A. J. Dickson, E. Thomas, R. E. M. Rickaby, P. Chapman, Z. Lu, Refining the planktic foraminiferal I/Ca proxy: Results from the Southeast Atlantic Ocean. Geochimica et Cosmochimica Acta 287, 318–327 (2020).

W. Lu, S. Wörndle, G. P. Halverson, X. Zhou, A. Bekker, R. H. Rainbird, D. S. Hardisty, T. W. Lyons, Z. Lu, Iodine proxy evidence for increased ocean oxygenation during the Bitter

Springs Anomaly. Geochem. Persp. Let., 53–57 (2017).

Z. Lu, B. A. A. Hoogakker, C.-D. Hillenbrand, X. Zhou, E. Thomas, K. M. Gutchess, W. Lu, L. Jones, R. E. M. Rickaby, Oxygen depletion recorded in upper waters of the glacial Southern Ocean. Nat Commun 7, 11146 (2016).

Z. Lu, H. C. Jenkyns, R. E. M. Rickaby, Iodine to calcium ratios in marine carbonate as a paleo-redox proxy during oceanic anoxic events. Geology 38, 1107–1110 (2010).

J. L. Morford, S. R. Emerson, E. J. Breckel, S. H. Kim, Diagenesis of oxyanions (V, U, Re, and Mo) in pore waters and sediments from a continental margin. Geochimica et Cosmochimica Acta 69, 5021–5032 (2005).

R. Raiswell, D. S. Hardisty, T. W. Lyons, D. E. Canfield, J. D. Owens, N. J. Planavsky, S. W. Poulton, C. T. Reinhard, The iron paleoredox proxies: A guide to the pitfalls, problems and proper practice. American Journal of Science 318, 491–526 (2018).

S. W. Poulton, The Iron Speciation Paleoredox Proxy. Elements in Geochemical Tracers in Earth System Science, doi: 10.1017/9781108847148 (2021).

S. W. Poulton, D. E. Canfield, Development of a sequential extraction procedure for iron: implications for iron partitioning in continentally derived particulates. Chemical Geology 214, 209–221 (2005).

S. W. Poulton, D. E. Canfield, Ferruginous Conditions: A Dominant Feature of the Ocean through Earth's History. Elements 7, 107–112 (2011).

Poulton, S.W., Krom, M.D. and Raiswell, R. (2004) A revised scheme for the reactivity of iron (oxyhydr)oxide minerals towards dissolved sulfide. Geochimica et Cosmochimica Acta, 68 (18). pp. 3703-3715.

S. W. Poulton, R. Raiswell, The low-temperature geochemical cycle of iron: From continental fluxes to marine sediment deposition. American Journal of Science 302, 774–805 (2002).

N. Tribovillard, T. J. Algeo, F. Baudin, A. Riboulleau, Analysis of marine environmental conditions based onmolybdenum–uranium covariation—Applications to Mesozoic paleoceanography. Chemical Geology 324–325, 46–58 (2012).

N. Tribovillard, T. J. Algeo, T. Lyons, A. Riboulleau, Trace metals as paleoredox and paleoproductivity proxies: An update. Chemical Geology 232, 12–32 (2006).

G. T. F. Wong, P. G. Brewer, The marine chemistry of iodine in anoxic basins. Geochimica et Cosmochimica Acta 41, 151–159 (1977).

Data Tables

Table S1. $\delta^{13}C_{PDB}$, $\delta^{18}O_{PDB}$, and elemental concentrations.

Sample	Height	$\delta^{13}C_{V\text{-}PDB}$	$\delta^{18}O_{V\text{-}PDB}$	Al	Fe	Mo	U	Re	Re/Mo	Re/U
	m	‰	‰	wt%	wt%	ppm	ppm	ppb	10^{-3}	10^{-3}
1	0	-0.77	-5.44	0.22	0.29	3.07	0.72	0.46	0.15	0.65
2	0.9			0.10	0.13	0.56	0.40			
3	1.9	-0.78	-6.74		0.16	0.28				
4	2.9			0.16	0.14	0.89	0.43			
5	3.9	-0.84	-5.89		0.10	0.58	0.33			
6	4.9			0.02	0.08	0.40	0.36			
7	5.9	-0.62	-5.30	0.24	0.16	0.96	1.98			
8	6.9			0.04	0.09	0.31				
9	7.9	-0.82	-5.71	0.02	0.10	0.08	0.29			
10	8.9				0.09	0.58	0.40			
11	9.9	0.43	-5.45	0.71	0.32	0.29	1.42			
12	11.1				0.14	0.35	0.66			
13	11.6	-0.08	-6.09		0.22	0.34	0.58			
14	12.6				0.14	0.31	0.70			
15	13.6	-0.13	-6.11		0.18	0.21	0.44			
16	14.8			0.02	0.10	0.50	0.47			
17	15.7	-0.22	-5.89		0.14	0.16	0.44			
18	16.7			0.06	0.14	0.17	0.49			
19	17.8	0.06	-6.12		0.10	0.46	0.37			
20	18.8				0.13	0.23	0.51			
21	19.5	-0.15	-5.38	0.14	0.42	0.36	0.76			
22	20.5			1.87	0.33	0.17	1.08			
23	22.5	-0.12	-6.37	0.88	0.40	0.16	0.80	0.35	2.24	0.44
24	23.9			0.06	0.27	0.08	0.37			
25	24.9	0.13	-6.46	1.83	0.86	0.95	0.79	0.67	0.70	0.85
26	25.8			0.19	0.50	0.73		0.49	0.66	
27	26.8	0.29	-6.31	1.59	0.77	0.57	0.41	0.42	0.74	1.02
28	27.8			0.02	0.27	0.27				
29	28.8	0.71	-6.40	0.24	0.76	0.58	0.29			
30	29.8			0.12	0.25	0.48	0.31	0.62	1.29	2.01
31	30.8	0.99	-6.43	0.23	0.55	0.44				
32	31.8			0.13	0.15	0.06				
33	32.8	1.09	-6.62	1.69	1.04	0.85	0.81	0.33	0.38	0.40
34	33.8			0.47	0.35	0.33	0.50	0.46	1.39	0.92
35	34.9	2.78	-5.79	0.64	0.44	0.39	0.62	1.11	2.85	1.80
36	35.9			1.32	1.46	1.22	1.03	0.97	0.79	0.93
37	36.9	0.79	-7.34	1.04	0.41	0.30	1.09	0.65	2.16	0.59
38	37.9			0.75	0.64	0.73	0.88	0.34	0.47	0.39
39	38.8	0.94	-5.81	1.14	0.43	0.51	1.23	0.33	0.64	0.26

40	39.9			0.09	0.59	1.57	0.67	0.35	0.22	0.52
41	40.9	0.89	-5.38	0.12	0.22	0.12	0.26			
42	42.7			0.28	0.15	2.27	0.33			
43	43.7	0.32	-5.61	0.65	0.32	0.21	0.36			
44	44.8			2.10	0.32	0.21	0.69	0.37	1.71	0.53
45	46.1	0.15	-5.86	0.17	0.78	0.78	0.39	0.34	0.43	0.86
46	47.1			0.79	0.33	0.31	0.68			
47	48.2	-0.49	-6.53	2.21	0.20	0.18	0.99	0.32	1.80	0.32
48	49.2			0.31	0.35	0.20	0.53	0.32	1.60	0.60
49	50.2	-0.31	-6.13	0.41	0.20	0.23	0.52	0.38	1.68	0.74
50	51.2			0.19	0.23	0.21	0.33	0.32	1.57	0.98
51	51.9	-0.85	-6.04	1.55	0.68	0.78	0.96	0.36	0.46	0.38
52	52.9			1.67	0.51	0.92	2.47	0.36	0.39	0.14
53	53.9	-0.13	-6.28	0.91	0.45	0.59	0.80			
54	54.9			0.28	0.51	0.53	0.45			
55	55.9	-0.05	-6.07	0.19	0.26	0.40	0.56			
56	56.9			0.27	0.32	0.40	0.45			
57	57.9	-0.09	-6.06	0.49	0.80	1.12	0.43			
58	58.9			0.69	0.34	0.32	0.29			
59	59.9	-0.08	-5.89	0.37	0.64	2.20	0.67	0.40	0.18	0.60
60	60.9			0.50	0.54	1.25	1.57	0.49	0.40	0.32
61	61.9	-0.21	-5.75	1.10	0.40	1.46	0.92			
62	62.9			0.27	0.36	0.37	1.04			
63	63.9	-0.03	-6.19	2.36	0.57	0.90	4.10	1.42	1.58	0.35
64	64.0			0.26	0.74	1.44	2.53			
65	65.0	-0.71	-6.73	1.59	0.61	2.28	9.94	1.14	0.50	0.12
66	66.0			0.61	1.09	1.13	1.53	0.46	0.41	0.30
67	67.0	-0.86	-6.64		0.26	0.20				
68	68.0			0.14	0.32	0.16	0.24			
69	69.0	-0.88	-6.21	0.98	0.33	0.28	0.43			
70	70.0			1.74	0.49	0.27	0.94			
71	71.0	-0.78	-6.15	1.12	0.42	1.35	2.95	1.68	1.24	0.57
72	72.6			2.35	1.04	0.73	2.01	0.35	0.48	0.18
73	73.6	-1.36	-5.92	0.58	0.20	0.47	0.32			
74	74.6			1.51	1.26	1.64	0.49	0.55	0.33	1.11
75	75.6	-0.98	-6.28							
76	77.3			0.28	3.11	6.08	1.78	0.78	0.13	0.44
77	78.3			2.80	0.30	0.50	0.75			

290 **Table S2. I/(Ca + Mg), Fe speciation data and enrichment factors.**

Sample	Height (m)	TOC wt%	I/(Ca+Mg) µmol/mol	Fe_{HR}/Fe_T	Fe_{PY}/Fe_{HR}	Mo_{EF}	U_{EF}	Re_{EF}
1	0.0	0.0145	0.26			3.69	1.25	2.83
2	0.9	0.0147				1.49	1.14	
3	1.9		0.21			1.25		
4	2.9	0.0090				1.77	1.14	
5	3.9	0.0179	0.22			1.51	1.12	
6	4.9	0.0286				1.36	1.13	
7	5.9	0.0141	0.26			1.82	1.72	
8	6.9	0.0059				1.27		
9	7.9	0.0065	0.23			1.07	1.11	
10	8.9	0.0120				1.51	1.15	
11	9.9	0.0189	0.31			1.17	1.45	
12	11.1	0.0143				1.31	1.25	
13	11.6	0.0126	0.22			1.30	1.22	
14	12.6	0.0151				1.27	1.27	
15	13.6	0.0095	0.20			1.19	1.17	
16	14.8	0.0247				1.44	1.18	
17	15.7	0.0182	0.20			1.14	1.17	
18	16.7	0.0173				1.14	1.18	
19	17.8		0.19			1.41	1.14	
20	18.8	0.0294				1.21	1.19	
21	19.5	0.0143	0.22			1.30	1.27	
22	20.5	0.0375				0.92	1.18	
23	22.5	0.0395	0.40			1.03	1.20	2.29
24	23.9	0.0440				1.07	1.13	
25	24.9	0.0684	0.33	0.56	0.022	1.62	1.07	3.46
26	25.8	0.0149				1.62		2.92
27	26.8	0.0128	0.22	0.63	0.021	1.31	0.96	2.49
28	27.8	0.0088				1.24		
29	28.8	0.0138	0.19	0.73	0.014	1.48	1.08	
30	29.8	0.0105				1.41	1.10	3.47
31	30.8	0.0097	0.22	0.64	0.011	1.36		
32	31.8	0.0118	0.25			1.04		
33	32.8	0.0190	0.18	0.91	0.008	1.55	1.10	2.09
34	33.8	0.0175	0.23			1.23	1.13	2.78
35	34.9	0.0131	0.27			1.27	1.16	5.38
36	35.9	0.0158	0.28	0.50	0.242	1.92	1.23	4.70
37	36.9	0.0197	0.27			1.14	1.28	3.45
38	37.9	0.0234	0.23	0.66	0.038	1.55	1.24	2.28
39	38.8	0.0199	0.24			1.31	1.33	2.16
40	39.9	0.0197		0.62	0.034	2.38	1.24	2.37
41	40.9	0.0112	0.22			1.09	1.08	

42	42.7	0.0186				2.97	1.09	
43	43.7	0.0128	0.22			1.11	1.06	
44	44.8	0.0147				0.93	1.00	2.21
45	46.1	0.0155	0.20	0.70	0.023	1.67	1.13	2.34
46	47.1	0.0202				1.18	1.16	
47	48.2	0.0128	0.22			0.88	1.10	2.00
48	49.2	0.0124				1.14	1.16	2.24
49	50.2	0.0095	0.21			1.15	1.15	2.48
50	51.2	0.0106				1.16	1.10	2.27
51	51.9	0.0259	0.21	0.57	0.044	1.50	1.17	2.25
52	52.9	0.0340		0.84	0.033	1.60	1.73	2.22
53	53.9	0.0156	0.20			1.41	1.19	
54	54.9	0.0166		0.68	0.034	1.44	1.14	
55	55.9	0.0110	0.20			1.33	1.19	
56	56.9	0.0082				1.32	1.14	
57	57.9	0.0225	0.20	0.64	0.012	1.93	1.10	
58	58.9	0.0099				1.20	1.02	
59	59.9	0.0113	0.18	0.62	0.013	2.90	1.21	2.57
60	60.9	0.0186		0.78	0.012	2.04	1.53	2.92
61	61.9	0.0213	0.24			2.16	1.21	
62	62.9	0.0130				1.30	1.36	
63	63.9	0.0531	0.23	0.59	0.055	1.50	2.27	6.38
64	64.0	0.0882		0.62	0.015	2.24	1.93	
65	65.0	0.0027	0.20	0.64	0.060	2.82	4.58	5.38
66	66.0	0.0124		0.79	0.005	1.92	1.51	2.78
67	67.0	0.0167	0.18			1.18		
68	68.0	0.0155				1.12	1.07	
69	69.0	0.0245	0.20			1.13	1.04	
70	70.0	0.0086				1.02	1.14	
71	71.0	0.0171	0.21			2.06	1.98	7.57
72	72.6	0.0090		0.60	0.001	1.36	1.48	2.12
73	73.6	0.0090	0.18			1.35	1.05	
74	74.6	0.0139		0.76	0.006	2.26	1.00	3.00
75	75.6	0.0150	0.17					
76	77.3	0.0524		0.77	0.001	6.35	1.64	4.08
77	78.3	0.0031				1.09	0.94	2.83